ARTICLE
Traditional Medicine Research 2024;9(10):56. https://doi.org/10.53388/TMR20240109001

Synthesis of chitosan oligosaccharide selenium and its antitumor activity

Yu-Mei Chen Yan[1#], Yu Chen[1#], Yin-Yin Li[1], Yue Bai[1], Yang Dong[1], Bing-Qiang Zhang[2, 3], Meng-Meng Chen[2, 3], Xi-Feng Zhang[1], Jing Liu[4*]

[1]College of Veterinary Medicine, Qingdao Agricultural University, Qingdao 266100, China. [2]Qingdao Restore Biotechnology Co., Ltd., Qingdao 266111, China. [3]Key Laboratory of Cancer and Immune Cells of Qingdao, Qingdao 266111, China. [4]Analytical & Testing Center of Qingdao Agricultural University, Qingdao 266100, China.

[#]These authors contributed equally to this work and are co-first authors for this paper.
[*]**Correspondence to:** Liu Jing, Analytical & Testing Center of Qingdao Agricultural University, No. 700, Changcheng Road, Chengyang District, Qingdao 266100, China. E-mail: liujingandlele@163.com.

Author contributions
Liu J designed the study and managed funding. Chen Yan YM and Chen Y performed the bioinformatic analysis. Li YY, Bai Y and Dong Y performed the experiments. Zhang BQ, Chen MM and Zhang XF discussed the manuscript. All authors drafted and approved the final manuscript.

Competing interests
The authors declare no conflicts of interest.

Acknowledgments
This work was supported by Localization of oxygen radicals and enzymes in bivalve haemocytes to Jing Liu (20230058, 6602423063).

Peer review information
Traditional Medicine Research thanks all anonymous reviewers for their contribution to the peer review of this paper.

Abbreviations
COS, chitosan oligosaccharide; COSSe, chitosan oligosaccharide selenium; CCNA1, cyclin A1; CON, Control; Na_2SeO_3, sodium selenite; UV, UV-visible spectroscopy; FTIR, Fourier transform infrared spectroscopy; CD, circular dichroism; SEM, scanning electron microscopy; TEM, transmission electron microscopy; XRD, X-ray diffraction; GO, Gene Ontology; KEGG, Kyoto Encyclopedia of Gene and Genome; DEGs, differentially expressed genes.

Citation
Chen Yan YM, Chen Y, Li YY, et al. Synthesis of chitosan oligosaccharide selenium and its antitumor activity. *Tradit Med Res*. 2024;9(10):56. doi: 10.53388/TMR20240109001.

Executive editor: Jing-Yi Wang.
Received: 09 January 2024; **Accepted:** 14 April 2024; **Available online:** 17 April 2024.

Abstract
Background: Polysaccharides have various biological activities; the complexation of polysaccharides with trace element ions can produce synergistic effects, improving the original biological activities of sugars and trace elements. **Methods:** The preparation process of chitosan oligosaccharide selenium (COSSe) was optimized by the response surface method, followed by a detailed analysis of the resultant compound's characteristics. The anti-cancer activity of COSSe was studied using the human ovarian cancer cell line SKOV3 as a cell model. **Results:** The prepared COSSe response surface was well predicted, indicating successful chitosan oligosaccharide binding with selenium. Response surface method analyses identified the optimal synthesis conditions for COSSe: the reaction time of 5.08 h, the reaction temperature of 71.8 ˚C, and mass ratio (Na_2SeO_3: chitosan oligosaccharide) of 1.02. Under the optimal conditions, the final product, the selenium content, reached 1.302%. The results of cell experiments showed that COSSe significantly inhibited SKOV3 proliferation in a concentration-dependent manner. RNA-seq results showed that chitosan oligosaccharide and COSSe significantly modulated the expression of genes' DNA metabolic processes and cell cycle in SKOV3 cells. Gene enrichment analysis showed the inhibition of the cell cycle, and the results of flow cytometry showed that SKOV3 cells increased in the S phase and decreased in the G2/M phase, with a noted suppression in the protein expression of cyclin-dependent kinase 2 (CDK2) and cyclin A1 (CCNA1). **Conclusion:** COSSe has a stronger effect than chitosan oligosaccharide, leading to the arrest of the cell cycle in the S phase. Thus, COSSe may be an effective candidate for the treatment of ovarian cancer.

Keywords: chitosan oligosaccharide; chitosan oligosaccharide selenium; ovarian cancer; SKOV3; RNA-seq

Highlights

The prepared chitosan oligosaccharide selenium (COSSe) response surface was well predicted. Chitosan oligosaccharide (COS) and COSSe can inhibit the gene and protein expression of cyclin-dependent kinase 2 (CDK2) and cyclin A1 (CCNA1), resulting in the blockage of SKOV3 cell cycle in S phase, and further inhibiting the proliferation of SKOV3 cells. Moreover, COSSe have a stronger inhibitory effect.

Medical history of objective

Chitosan is originally derived from chitin. As early as in ancient times, people began to utilize the shells of crustaceans. The application history of chitin can be traced back to the records of crab shells in Li Shi-Zhen's medical book "*Compendium of Materia Medica*" (1578 C.E.), which pointed out their effectiveness in breaking up blood stasis and relieving accumulation. In 1811 C.E., French scientist H. Braconnot first isolated chitin from mushrooms, which was the earliest scientific understanding of chitin by humans. Subsequently, research on chitin and chitosan gradually unfolded. By the 20th century, significant progress had been made in the preparation and application research of COS. Due to its good water solubility and high biological activity, COS has shown broad application prospects in the fields of medicine, health care products, and agriculture. After 2000 C.E., China also launched various health food products containing COS. Modern research has shown that COS can enhance the body's immune function, lower blood pressure and blood lipids, promote the repair of injured tissues, and possess excellent anti-tumor activity.

Background

Polysaccharides are carbohydrate substances with complex molecular structures, which are formed by condensation of multiple monosaccharide molecules and loss of water. Polysaccharides are widely distributed in nature and play key roles in biological systems [1]. Polysaccharide compounds, which are widely found in the cell membranes and cell walls of animals, plants, and microbes, are one of the four basic materials of life. Studies have shown that polysaccharides have various biological activities such as anti-oxidation, anti-aging, antitumor, immune regulation, organ protection, and so on. Therefore, polysaccharides have attracted great attention from scholars in the fields of food science, medicine, and biology [2]. The chemical structure exhibited by polysaccharides provides the material basis for their biological activities. However, the biological activities of naturally obtained polysaccharides may not reach the desired effects and limit their further application. Possible structural modifications of polysaccharides may enhance their properties, which has become a focus of research. It has been reported that complexes formed by polysaccharides with certain metal and non-metal ions are more special in structure and have enhanced biological activities. It is one of the indispensable components of living organisms and has been widely used in medicine and functional food [3].

Functional polysaccharides, present in various traditional Chinese medicine, have attracted increasing attention in scientific research in recent years [4]. Moreover, the development of metal ion-modified carbohydrate compounds is also extremely rapid, and more and more metal elements and carbohydrate compounds are involved in the reaction. Polysaccharide selenium has attracted much attention due to its high antitumor activity [5]. Selenium is a necessary trace element in the human body and plays an important role in many physiological processes [6]. Selenium has inorganic and organic forms in nature. Inorganic selenium, commonly found in acid salts and selenite, can easily accumulate to toxic levels in the body and potentially induce mutations [7]. Organic selenium is mainly found in selenoproteins and selenopolysaccharides in animals and plants. Compared with inorganic selenium compounds, organic selenium compounds have higher biological activity and can be better absorbed by the human body [8]. Selenium deficiency causes diseases such as tumors and cataracts [9]. Therefore, selenium polysaccharides, which have the advantages of both selenium and polysaccharide, have attracted more and more attention from scholars. As a new functional polysaccharide, selenium polysaccharide exhibits multiple functions, including anti-oxidation, antitumor, immune regulation, hypoglycemic, liver protection, neuroprotection, anti-heavy metal, and so on [10]. There are also numerous reports on its structure and biological activity. At present, natural selenium polysaccharides successfully obtained by biological transformation and modification methods include *Ganoderma lucidum* selenium polysaccharide, shiitake mushroom selenium polysaccharide, spirulina selenium polysaccharide, ruo leaf selenium polysaccharide, garlic selenium polysaccharide, and auricularia selenium polysaccharide. Due to the biological functions of selenium and polysaccharides, the combination of selenium and polysaccharide can produce more biological effects, be helpful for human body absorption use, have small side effects, and be more safe for the human body [10]. Studies have shown that polysaccharides with higher selenium content have stronger antitumor and neuroprotective activities [5, 11].

In this study, COS and sodium selenite (Na_2SeO_3) were used as raw materials, and the preparation process of COSSe was optimized by the response surface method. The characterization of COSSe was conducted through various analytical techniques, including UV-visible spectroscopy (UV), Fourier transform infrared spectroscopy (FTIR), circular dichroism (CD), scanning electron microscopy (SEM), transmission electron microscopy (TEM), and X-ray diffraction (XRD). Furthermore, we used the human ovarian cancer cell line SKOV3 as a cell model to study the anti-cancer activity of COSSe.

Experimental methods

Preparation of COSSe

Precisely weigh the appropriate amount of COS dissolved in dilute nitric acid solution, and add the appropriate amount of Na_2SeO_3 and barium chloride for a reaction in a solid water bath. After the reaction, add the appropriate amount of anhydrous sodium sulfate to remove unreacted barium chloride. The above test solution was centrifuged to deprecipitate, and the supernatant was dialyzed for 20 h. After that, three times the volume of 95% ethyl alcohol was added to precipitate for 12 h at 4 °C and then centrifuged. The centrifuged precipitate was put into a freeze-drying oven to dry, which was to obtain the finished product of COSSe [12].

The analysis of selenium

Using the theory of o-phenylendiamine spectrophotometry to detect the selenium content o-phenylendiamine with selenium can form stable chelate, which has the characteristic absorption peak [13].

Determination of COSSe and establishment of selenium standard curve. Precision weighing 50 mg Na_2SeO_3 reacted it with 3 mL of mixed acid, volume the mixture to 50 mL with water for later use. The selenium reference solution was prepared by taking 1 mL of the above solution in a 250 mL volumetric flask. Take 1 mL, 3 mL, 4 mL, 5 mL, 6 mL, 8 mL, 10 mL, 12 mL of selenium control solution and add 25 mL of ddH_2O each. The above solution with ammonia the PH to 2, and the solution of o-phenylenediamine in 2 h. The standard curve of selenium can be obtained by measuring the absorbance of the eight sets of data at 334 nm.

Determination of selenium content in COSSe. This research uses the spectrophotometric method to determine the selenium content. The specific procedure is as follows: dissolve 20 mg of COSSe in acidic conditions, adjust the pH to 2 with ammonia, and then add a 1% solution of o-phenylenediamine. Make the mixture stand for 2 h, followed by extraction with xylene. Dilute the extracted solution to a volume of 10 mL using dimethylbenzene xylene. Finally, measure the absorbance of the COSSe reaction liquid at 334 nm. The selenium content of COSSe can be calculated by substituting the measured

absorbance into the following Equation (1):

$$Y = (X - 0.00631) \div 0.1467 \quad (1)$$

Type: X for absorbance, Y for selenium content.

Optimization of oligosaccharide selenium preparation technology

Single factor experiment. Selected reaction temperature (°C, A), the mass ratio (Na_2SeO_3:COS, B), and time (h, C) are the three factors that will be used to complete the single-factor experiment. Through each sample, absorbance spectrophotometry integrates all the absorbance of the sample to see the best single-factor conditions.

Response surface methodology design and validation of COSSe preparation. Based on the results of the single-factor experiment, a Box-Behnken Design was implemented. The experimental data were analyzed using Design-Expert 8.0.6.1 software to determine the best synthesis conditions. The response surface will give the fitting equation and the best process. Under these conditions, five groups of parallel experiments will be carried out to verify and calculate the deviation rate. The Equation (2) is as follows:

$$\text{Deviation Rate} = \frac{\text{Actual Value} - \text{Theoretical Value}}{\text{Theoretical Value}} \times 100\% \quad (2)$$

Characterization analysis of COS and COSSe

UV analysis. 0.1 g COS and COSSe were precisely weighed and fully dissolved in 1 mL ddH_2O and centrifuged at 5,000 r/min for 5 min to ensure the clarity of the supernatant. The UV spectra of these samples were scanned across a wavelength range of 200 to 800 nm.

FTIR analysis. The mixture of 3 mg COS and COSSe with 100 mg potassium bromide was ground thoroughly and placed into a circular mold under pressure (5–10 t/cm^2) for about 1 min to press the fine powder into a transparent circular sheet. These samples were characterized by FTIR spectroscopy (PerkinElmer, Spectrum 400, Waltham, MA, USA) with a scanning wavelength range of 4,000 to 500 cm^{-1}.

CD analysis. Samples of COS and COSSe at 1 mg/mL were scanned and analyzed with a CD spectrometer (Jasco Inc., Easton, MD, USA) at room temperature. The scanning wavelength ranged from 190 nm to 300 nm, the scanning speed was 50 nm/min, and the sensitivity was 2 MB/cm.

SEM analysis. Scanning electron microscopy (Hitachi, Tokyo, Japan) was used to observe the morphological characteristics of the specimens. These samples were dried and evenly dispersed on copper sheets. Field emission scanning electron microscopy was used.

TEM analysis. The pore structure of COS and COSSe samples was characterized and analyzed using a transmission electron microscope (Tecnai F20, FEI, Hillsboro, OR, USA). For the field emission experiments, the test voltage is 200 kV.

XRD analysis. XRD analysis was employed to ascertain the crystallinity of COS and COSSe (D2 PHASER, Bruker AXS, Karlsruhe, Germany). The voltage was 40 kV, the current was 40 Ma, and the scanning was performed at 2θ = 5–60 ° with a scanning speed of 4 °/min.

Cell experiment

Cell culture. The human ovarian cancer cell lines SKOV3 (JN16355, Jining Shiye, Shanghai, China) were cultured in DMEM (PM150210, Procell, Wuhan, China) + 10% fetal Bovine Serum (Capricorn Scientific, Ebsdorfergrund, Germany) + 1% penicillin-streptomycin-amphotericin B sterile solution (P7630, Solarbio, Beijing, China), and incubated at 37 °C in a humidified, 5% CO_2 atmosphere.

Cell viability. The effects of COS and COSSe on SKOV3 cell viability were determined using the MTT kit (M1020, Solarbio, Beijing, China). According to the instructions, cells were cultured in DMEM medium containing COS and COSSe at concentrations of 100 μg/mL, 200 μg/mL, 300 μg/mL, 400 μg/mL, and 500 μg/mL for 24 h in 96 wells plate. After that, MTT solution was added and treated for 4 h. The supernatant was then removed, and formazan solution was added; the mixture was shaken at a low speed at room temperature for 10 min. Then, the plate was put into an ultra-sensitive multifunctional microplate detector (Bio Tek, Winooski, VT, USA), and the absorbance of each well at the wavelength of 490 nm was detected.

Cell multiplication. BeyoClick EdU cell proliferation and Alexa Fluor 555 (EdU-555) kit (C0075S, Beyotime, Shanghai, China) were used to test cell multiplication. Cells were treated for 24 h with DMEM medium containing COS and COSSe at the concentration of 100 μg/mL. Press kits instruction training EdU, fix penetration, then add the reaction liquid. After sealing, they were observed and photographed under a fluorescence microscope (Olympus, Tokyo, Japan). During the incubation period, DNA replication SKOV3 showed red fluorescence, and the nuclei showed blue fluorescence. The red-blue fluorescence ratio was calculated as the basis for proliferation rates using ImageJ (version 1.53k).

Cell cycle. Cell cycle and apoptosis analysis kit (C1052, Beyotime, Shanghai, China) were used to test cell cycle. Cells were treated for 24 h with DMEM medium containing COS and COSSe at the concentration of 100 μg/mL. The collected cells were resuspended in precooled PBS and later fixed with precooled 70% ethanol for more than 24 h. Then, cells were stained with propidium iodide and detected by flow cytometry (Becton Dickinson, Franklin Lakes, NJ, USA). Using FlowJo V10 software to analyze the data.

RNA-seq. The SKOV3 cells were cultured for 24 h using a DMEM medium containing COS and COSSe at the concentration of 100 μg/mL. The Hiseq 4000 platform of Novogene (Beijing, China) was used for mRNA sequencing. Sequence data were controlled, cropped, and filtered with fast (version 0.19.5) [14]. High-quality reads were aligned with the human reference genome (GRCh38) using the STAR algorithm. The threshold of differentially expressed mRNA $\log_2$ (fold change) ≥ 1, P value < 0.05. The expression of each gene and transcript was calculated using features (version 1.6.3). Gene Ontology (GO) and Kyoto Encyclopedia of Gene and Genome (KEGG) analysis of enrichment is the https://www.bioinformatics.com.cn online platform for data analysis and visualization. Using the STRING database (https://string-db.org/), build the differentially expressed genes (DEGs) between protein and protein interaction network by Cytoscape (http://www.cytoscape.org/).

Western blotting. Cells were cultured for 24 h with DMEM medium containing COS and COSSe at the concentration of 100 μg/mL. Then, the collected cells were added with an appropriate amount of RIPA lysis buffer and phenylmethanesulfonyl fluoride for total protein extraction. The sample proteins were separated by gel electrophoresis at a constant pressure of 100 v and then transferred to a PVDF membrane at a constant pressure of 200 mA. Then, it was blocked for 4 h at room temperature and incubated with primary antibodies (glyceraldehyde-3-phosphate dehydrogenase (GAPDH), CDK2, CCNA1, ABclonal, Wuhan, China) overnight in a 4 °C refrigerator. The primary antibody incubation was followed by elution with TBST for 10 min and repeated 3 times, followed by incubation with secondary antibody (S0001, Affnity, Liyang, China) (1:2,000) for 1.5 h at room temperature, and finally, protein signals were detected with a BeyoECL plus kit (P0018M, Beyotime, Shanghai, China) [15]. Blots were analyzed using ImageJ (version 1.53k) with GAPDH as the reference protein.

Statistical methods. The statistical analysis was performed with GraphPad Prism software (v8.0.2, San Diego, CA, USA), and the significant difference was determined with a 2-tailed student's unpaired T-test. Comparisons were considered significant at $^{*}P < 0.05$ and $^{**}P < 0.01$.

Results

Optimization of COSSe synthesis technology

Establishment of the standard curve. The standard curve for selenium was derived based on the absorbance of COS at 334 nm. This resulted in the Equation (3):

$$Y = 0.1467X + 0.00631 \quad (3)$$

with a coefficient of determination (R^2) of 0.991 (Figure 1A). A linear

relationship between the absorbance (Y) and the concentration of selenium ions (X) was observed within the concentration range of 0 to 4.8 μg/mL.

Single factor experiment. The results of the effect of reaction time, mass ratio (Na_2SeO_3:COS), and reaction temperature on Se content are shown in Figure 1B–1D using the control variable method. When a single factor the reaction time is 5 h, the mass ratio (Na_2SeO_3:COS) is 1.0, the reaction temperature is 70 °C, the highest selenium content of COSSe.

RSM of COSSe synthesis. Combined with the results of single factor experiments, response surface methodology experiments were designed based on the Box-Benhnken experimental principle. Three factors were considered: reaction time, mass ratio (Na_2SeO_3:COS), and reaction temperature. The selenium content was the response variable. Using Design-Expert software, 17 sets of response surface experiments were devised. The results are presented in Table 1.

The ANOVA of the response surface is shown in Table 2. According to the variance and significance test, the *P*-value of the Model is 0.0004, which is extremely significant, indicating the feasibility of the established response surface model. The R^2 of the Model is 0.9605, and its value is greater than 0.95, indicating that the Model is reliable. The Adj R-Squared (R^2_{Adj}) = 0.9097 indicates that the Model can predict 90.97% of the response value. A ratio of Adeq Precision greater than 4 is desirable. The signal-to-noise ratio of this Model is 12.408, which means that the signal is sufficient. This Model can be used to analyze and predict the selenium content of COSSe.

The Origin software was used to draw the 3D Surface diagram and Contour diagram of COSSe, and the results are shown in Figure 1E–1G. The ellipse in the contour plot indicates that there is a strong interaction between various factors, which has a significant effect on the synthesis of COSSe.

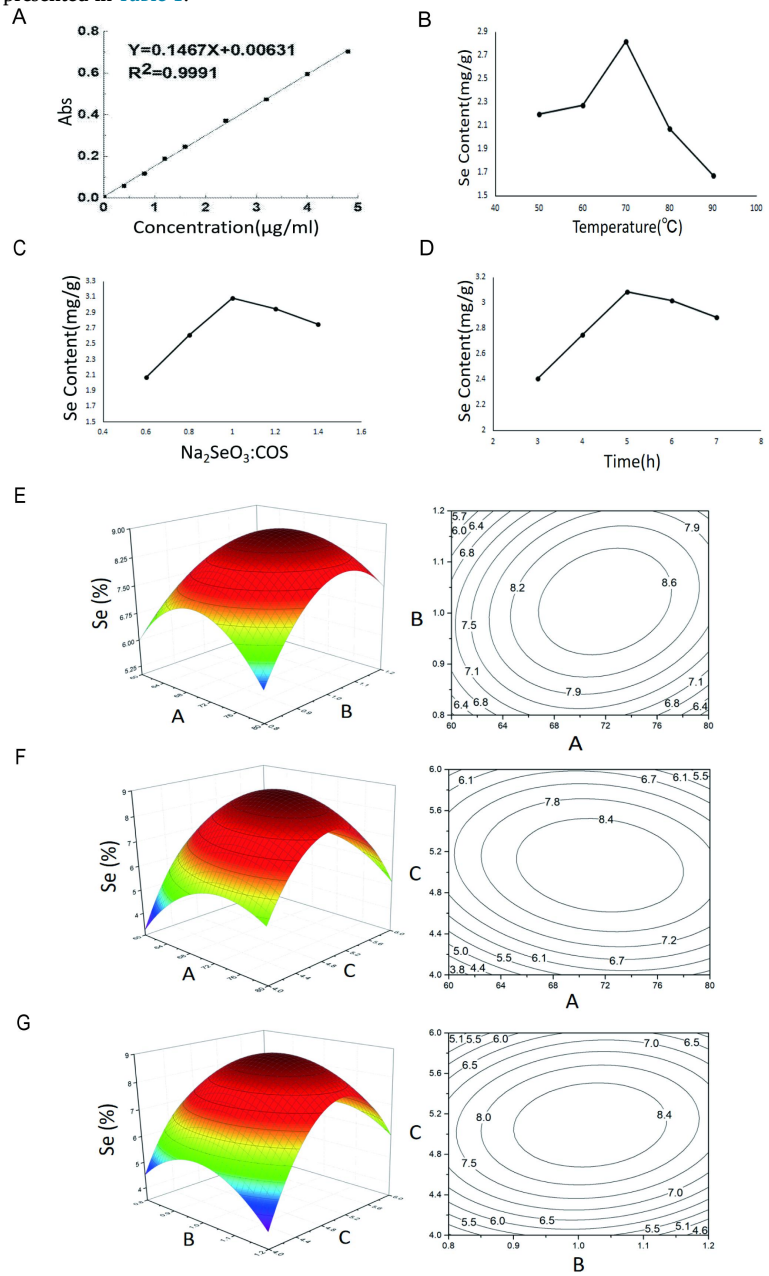

Figure 1 Single factor experiment and response surface optimization of the preparation of COSSe. (A) Se standard curve. (B) Effect of reaction temperature on Se content. (C) Effect of mass ratio of Na_2SeO_3 and COS on Se content. (D) Effect of reaction time on Se content. (E) Response surface and contour plot of temperature and mass ratio of Na_2SeO_3 and COS. (F) Response surface and contour plot of mass ratio of Na_2SeO_3 and COS and time. (G) Response surface and contour plot of temperature and time. A, temperature; B, mass ratio of Na_2SeO_3 and COS; C, time. COSSe, chitosan oligosaccharide selenium; COS, chitosan oligosaccharide.

Table 1 Box-behnken experiment design and results

Run	A-Temperature (°C)	B-Na_2SeO_3:COS	C-Time (h)	Se (%)
1	70.00	1.00	5.00	1.307
2	70.00	1.20	4.00	0.581
3	70.00	1.00	5.00	1.298
4	70.00	1.00	5.00	1.291
5	70.00	0.80	4.00	0.695
6	80.00	1.20	5.00	1.187
7	60.00	1.00	4.00	0.561
8	70.00	0.80	6.00	0.714
9	70.00	1.00	5.00	1.311
10	70.00	1.20	6.00	0.838
11	80.00	1.00	6.00	0.687
12	80.00	0.80	5.00	0.911
13	70.00	1.00	5.00	1.34
14	60.00	1.20	5.00	0.741
15	60.00	1.00	6.00	0.857
16	80.00	1.00	4.00	0.711
17	60.00	0.80	5.00	0.781

Taking the sample selenium content as the response value (Y), the regression Equation (4) obtained by fitting is as follows:

$$Y = -158.44625 + 1.99313 * A + 40.32500 * B + 29.62375 * C + 0.27000 * A * B - 0.054250 * A * C + 2.02500 * B * C - 0.013888 * A^2 - 34.15625 * B^2 - 2.73875 * C^2 \quad (4)$$

Table 2 ANOVA

Source	Sum of squares	DOF	Mean square	F-value	*P*-value
Model	59.16	9	6.57	18.92	0.0004
A-Temperature (°C)	1.81	1	1.81	5.22	0.0562
B-Na_2SeO_3:COS	0.34	1	0.34	0.99	0.3526
C-Time (h)	1.72	1	1.72	4.95	0.0614
AB	1.17	1	1.17	3.36	0.1096
AC	1.18	1	1.18	3.39	0.1083
BC	0.66	1	0.66	1.89	0.2118
A^2	8.12	1	8.12	23.37	0.0019
B^2	7.86	1	7.86	22.62	0.0021
C^2	31.58	1	31.58	90.88	< 0.0001
Residual	2.43	7	0.35		
Lack of fit	2.37	3	0.79	48.26	0.0013
Pure error	0.065	4	0.016		
Cor total	61.60	16			
$R^2 = 0.9605$	$R^2_{Adj} = 0.9097$		Adeq precisior = 12.408		

$P < 0.05$ was significant; $P < 0.01$ was highly significant. Na_2SeO_3, sodium selenite; COS, chitosan oligosaccharide.

The optimum process conditions, as predicted by the response surface, are a reaction time of 5.08 h, a reaction temperature of 71.8 °C, and a mass ratio (Na_2SeO_3 to COS) of 1.02. The predicted selenium content of the finished product is 1.302%. Five sets of parallel synthesis experiments conducted under these conditions yielded selenium contents of 1.269%, 1.261%, 1.258%, 1.260%, and 1.256%, respectively, with an average selenium content of 1.2508%. Compared with the predicted value of 1.302%, there was 96.1% agreement, and the deviation rate was 3.9%, which indicated that the prediction of the response surface was good.

Characterization analysis of COS and COSSe

UV assay. The comparison of COS and COSSe UV scanning patterns showed that the UV absorption at 300–400 nm was higher, which proved the presence of Se in the finished COSSe products (Figure 2A).

FT-IR assay. According to the FT-IR spectra, COS has characteristic absorption peaks typical of polysaccharides (Figure 2B). The broad peak at 3,417.4 cm^{-1} was the stretching vibration peak of polysaccharide O-H, 2,935.2 cm^{-1} was the stretching vibration absorption peak of polysaccharide C-H, and 1,627.7 cm^{-1} was the stretching vibration peak of polysaccharide carbonyl C=O. 1,430.9 cm^{-1} for polysaccharide carbonyl C-O stretching vibration peak, 1,145.5 cm^{-1} for polysaccharide hydroxy O-H bending vibration peak. The characteristic absorption peak of the polysaccharide in COSSe is

still evident and essentially identical to that of the unmodified COS. This indicates that the structure did not change greatly after the reaction of COS and COSSe, and the original properties of COS were maintained. However, the COSSe FT-IR spectra exhibit multiple distinctive absorption peaks between 1,000–2,000 cm^{-1} compared to COS, confirming the successful synthesis of COSSe.

CD assay. The CD assay of COS and COSSe in the range of 190–300 nm showed a decrease in peak values between 200–240 nm (Figure 2C). This phenomenon indicates that the synthesis of COSSe increases the asymmetry of the polysaccharide molecules, resulting in a conformational change.

XRD assay. XRD scanning results are shown in Figure 2D. COS has a series of sharp, intense characteristic diffraction peaks at 2θ = 10–40 °, consistent with its crystalline properties. In the case of the COSSe complex, the complex COSSe has sharp characteristic peaks at 2θ = 10–40 °, indicating that the selenium is dispersed in the COS molecules and the crystallite is reduced or disappeared.

SEM assay. Under the 100× SEM, photos show COS in spherical forms, different sizes and scattered distribution; the cross section appears relatively coarse (Figure 2E). COSSe at 100× electron microscopy appears with selenium attached to the surface of the fragmented COS (Figure 2F).

TEM assay. Compared with Figures 3A–3D, the percentage content of each element in COS and COSSe, both before and after, can be intuitively observed. The content of the carbon element is high, followed by the oxygen element. The content of Se in COSSe is about 1.17%, which is close to the concentration measured in the finished product.

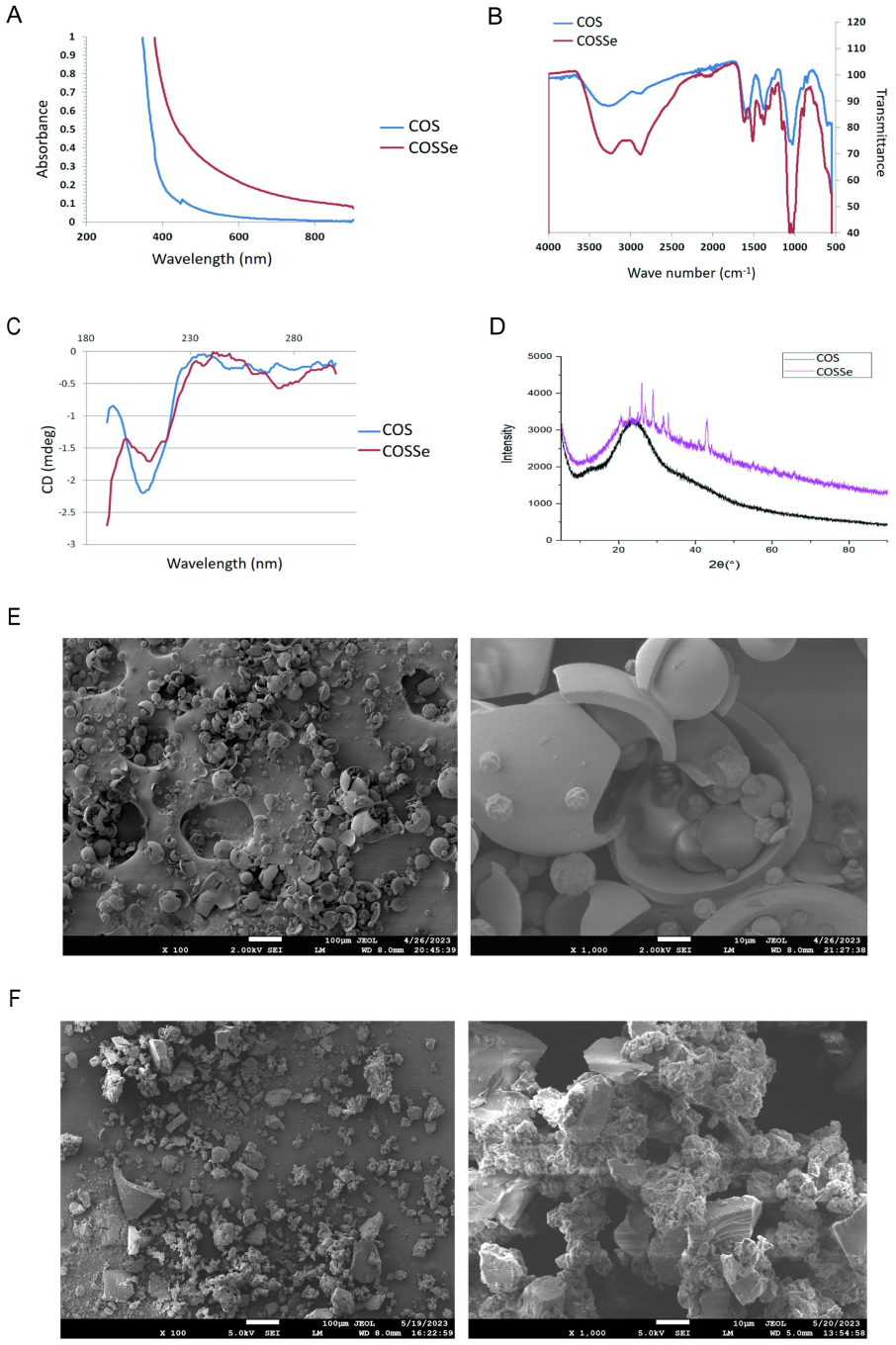

Figure 2 Spectroscopic characterization analysis and SEM of COS and COSSe. (A) UV spectra. (B) FTIR spectra. (C) CD spectra. (D) XRD analysis. (E) SEM images of COS. Bar = 100 μm, 10 μm. (F) SEM images of COSSe. Bar = 100 μm, 10 μm. COSSe, chitosan oligosaccharide selenium; COS, chitosan oligosaccharide.

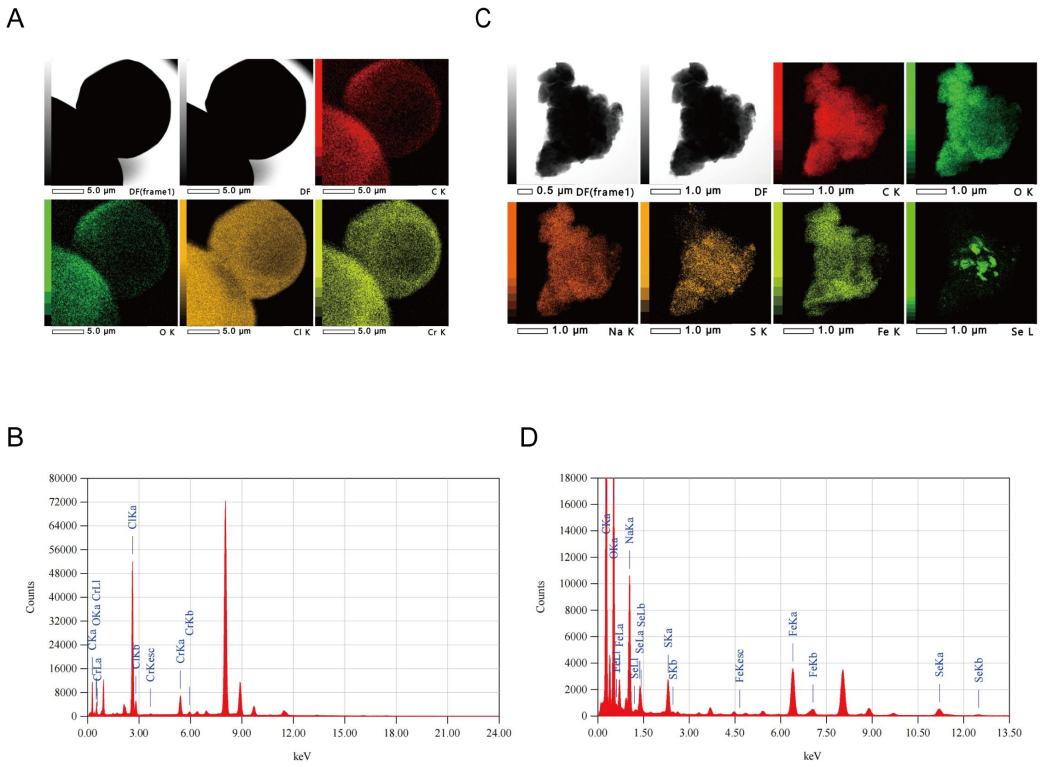

Figure 3 TEM analysis of COS and COSSe. (A) TEM images of COS. Bar = 5 μm. (B) Energy spectrum of COS. (C) TEM images of COSSe. Bar = 1 μm. (D) Energy spectrum of COSSe.

Exposure to COS and COSSe inhibited SKOV3 proliferation and hindered cell cycle progression

To investigate the impact of COS and COSSe on SKOV3 cells, an MTT assay was used to determine the effects of COS and COSSe on SKOV3 viability (Figure 4A). The results showed that both COS and COSSe significantly inhibited SKOV3 in a concentration-dependent manner, but COSSe had a stronger inhibitory effect than COS. Based on cell viability results, we treated SKOV3 with 100 μg/mL COS and COSSe for 24 h. The results showed significant differences in cell number and morphology of SKOV3 after 24 h of exposure to COS and COSSe compared to the control group (Figure 4B). EdU is a thymine DNA nucleoside analog; in the process of DNA synthesis, it can replace thymine DNA nucleotides and incorporate them into the new synthesis of DNA. Therefore, the proliferation ability of SKOV3 was examined using an EdU kit. The results showed that the proportion of edu-positive cells in the COS-treated group was not significantly different from that in the control group, while the proportion of edu-positive cells in the COSSe-treated group was significantly different from that in the control group (Figure 4B), further verifying the detection results of COSSe in MTT.

COS and COSSe exposure alters *SKOV3* mRNA expression

To clarify the mechanisms underlying the inhibition of SKOV3 proliferation by COS and COSSe exposure, mRNA expression levels were analyzed through transcriptional sequencing. The uniformity of the FPKM density distribution indicated the absence of outliers in the gene expression data, ensuring high accuracy in the data analysis (Figure 5A). PCA profiles showed that *SKOV3* gene expression was significantly altered after COS and COSSe treatment (Figure 5B). After we developed COS exposure to SKOV3, 1,040 genes were upregulated, and 558 genes were downregulated (Figure 5C). In contrast, COSSe exerted a more pronounced effect, with 1,706 genes upregulated and 1,046 genes downregulated (Figure 5D). In KEGG enrichment analysis, we found that both COS and COSSe affect the cell cycle of SKOV3, cellular senescence (Figure 6A). In GO: biological process (BP) enrichment analysis, we found that both COS and COSSe affect the ribonucleoprotein complex biogenesis, cytoplasmic translation, ribosome biogenesis, and other functions of SKOV3 (Figure 6B). We further performed functional enrichment analysis of COSSe versus COS group differential genes, and we found that it was associated with the DNA metabolic process and cell cycle (Figure 6C). Moreover, flow cytometry results of SKOV3 cells after COS and COSSe exposure showed a significant increase in the S phase and a significant decrease in the G2/M phase (Figure 7A). Western blotting results showed that the expression of SKOV3 cell cycle-related genes *CCNA1* and *CDK2* was decreased after exposure to COS and COSSe, especially COSSe (Figure 7B).

Discussion and conclusion

Trace elements, such as chromium, cobalt, copper, iodine, iron, manganese, molybdenum, selenium, and zinc, play a particularly important role in the normal life activities of animals. Most polysaccharides contain active groups such as the hydroxyl group, amino group, and negative oxygen group, which easily form complexes with a variety of metal ions and non-metal ions through chemical and physical adsorption to exert better biological effects. The complexation of polysaccharides and trace elements can produce synergistic effects, improve solubility, stability, and biological adaptability, and improve the original biological activities of polysaccharides and trace elements [10]. Studies have shown that codoginseng polysaccharide iron and pyro echinococcus polysaccharide iron have good metal ion chelation ability, which can scavenge DPPH and ABTS free radicals, increase the level of reactive oxygen species in human ovarian cancer cells, reduce mitochondrial membrane potential, and damage cell DNA [16, 17]. Tea tree mushroom selenium polysaccharide can increase the activities of superoxide dismutase, glutathione peroxidase, and total antioxidant activity in the serum of mice [18]. Astragalus zinc polysaccharide can improve insulin sensitivity and inhibit lipid oxidative stress in streptozotocin-induced type II diabetic rats [19]. In addition, a nano-carrier material based on *Angelica sinensis* polysaccharide has been synthesized to effectively enhance the proliferation inhibition activity of HepG2 cells [20].

In this study, COS and Na_2SeO_3 were used as raw materials to prepare COSSe, the surface optimization test was carried out, and the

response surface was well predicted, indicating a successful combination of COS and selenium. It has been shown that polysaccharides and trace element complexes exhibit higher biological activity compared to polysaccharides alone. *Poria cocos* has no significant inhibitory effect on ovarian cancer cells, but complexation with zinc ions can inhibit the proliferation of ovarian cancer cells at a lower concentration and induce cell apoptosis at a higher concentration [21]. Sargasso selenium polysaccharide exhibits a greater inhibitory effect on the α-glycosidase enzyme than the polysaccharide alone and the drug acarbose [22]. In the present study, we also confirmed that both COS and COSSe inhibited SKOV3 proliferation in a significantly concentration-dependent manner, and COSSe inhibited SKOV3 proliferation more strongly than COS.

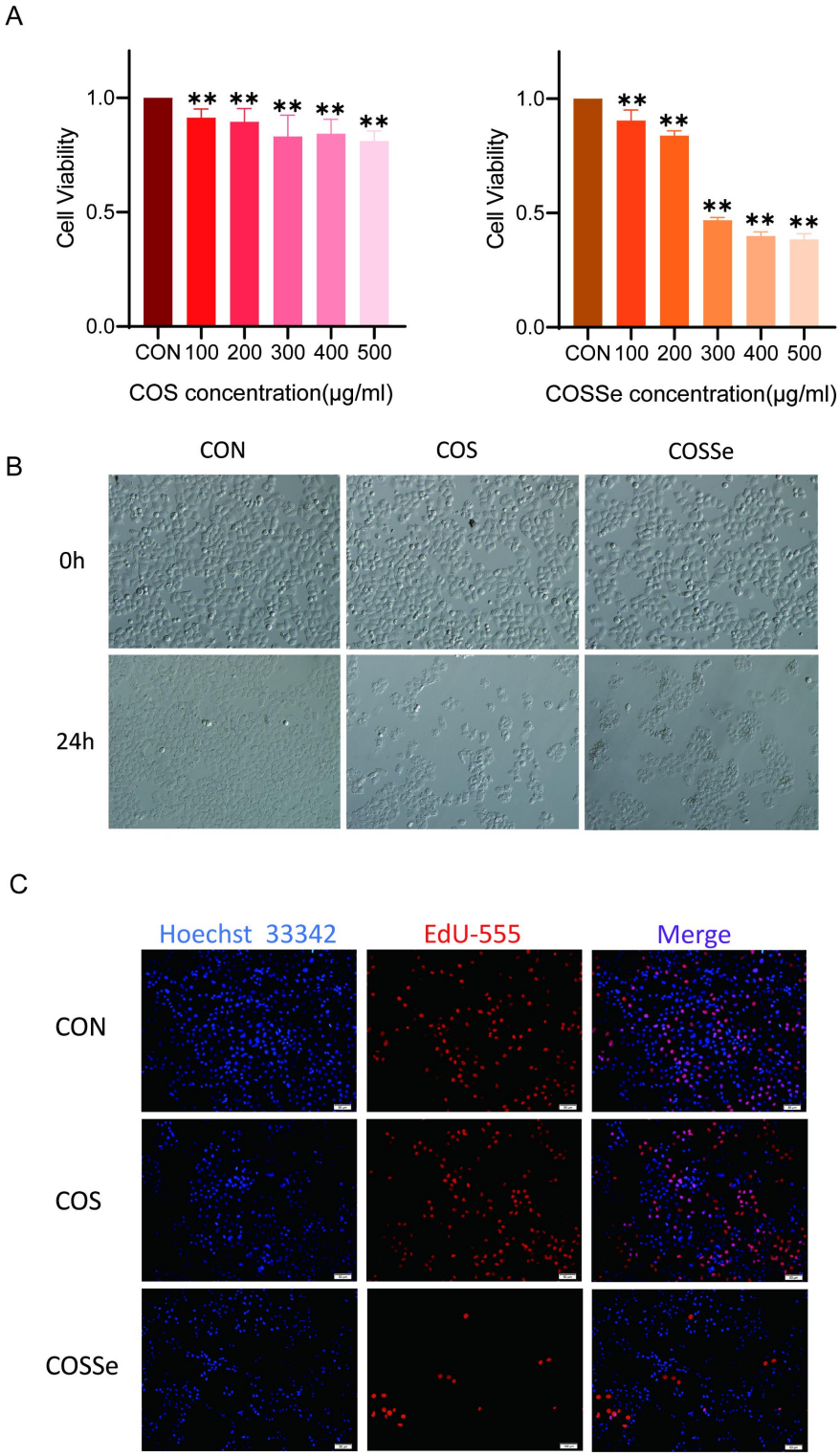

Figure 4 COS and COSSe inhibited SKOV3 proliferation. (A) Effects of different concentrations of COS and COSSe on the viability of SKOV3 cells. $^{*}P < 0.05$, $^{**}P < 0.01$ vs. the control group. (B) Representative images of SKOV3 treated with COS and COSSe for 0 h/24 h. Bar = 50 μm. (C) Immunofluorescence photos of EdU positive cells (red) and nuclei (blue) 24 h after COS and COSSe treatment. Bar = 50 μm. CON, Control; COSSe, chitosan oligosaccharide selenium; COS, chitosan oligosaccharide.

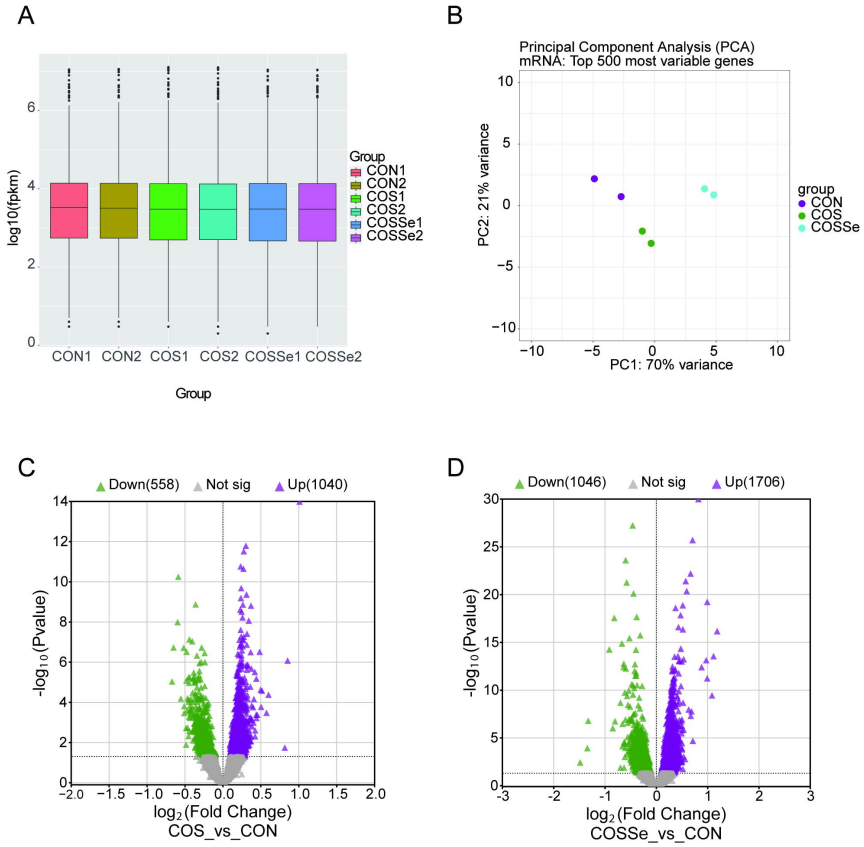

Figure 5 COS and COSSe alter SKOV3 transcriptional patterns. (A) Density profiles showed mRNA expression profiles in SKOV3 cells from CON, COS, and COSSe groups, respectively. (B) PCA based on mRNA. (C) Volcano plot of DEGs in COS versus CON groups. (D) Volcano plot of DEGs in COSSe versus CON groups. FPKM, fragments per kilobase per million; CON, Control; COSSe, chitosan oligosaccharide selenium; COS, chitosan oligosaccharide.

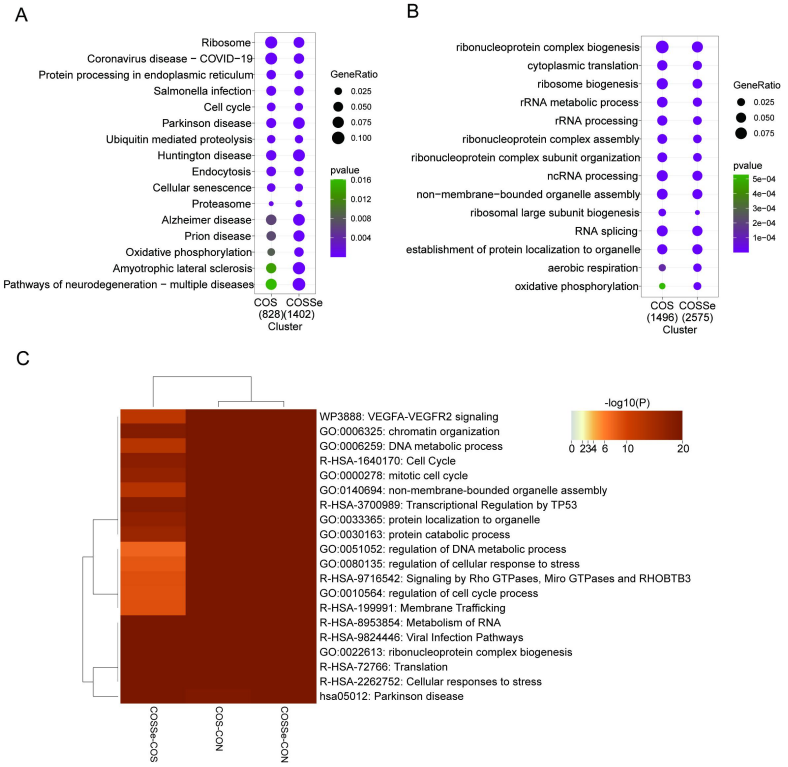

Figure 6 COS and COSSe alter the cell cycle of SKOV3. (A) KEGG enrichment analysis of differential genes in SKOV3 cells by COS and COSSe. (B) GO: BP enrichment analysis of differential genes in SKOV3 cells by COS and COSSe. (C) Metascape analysis of common enrichment pathways between COSSe and COS differential genes. CON, Control; COSSe, chitosan oligosaccharide selenium; COS, chitosan oligosaccharide; GO, Gene Ontology.

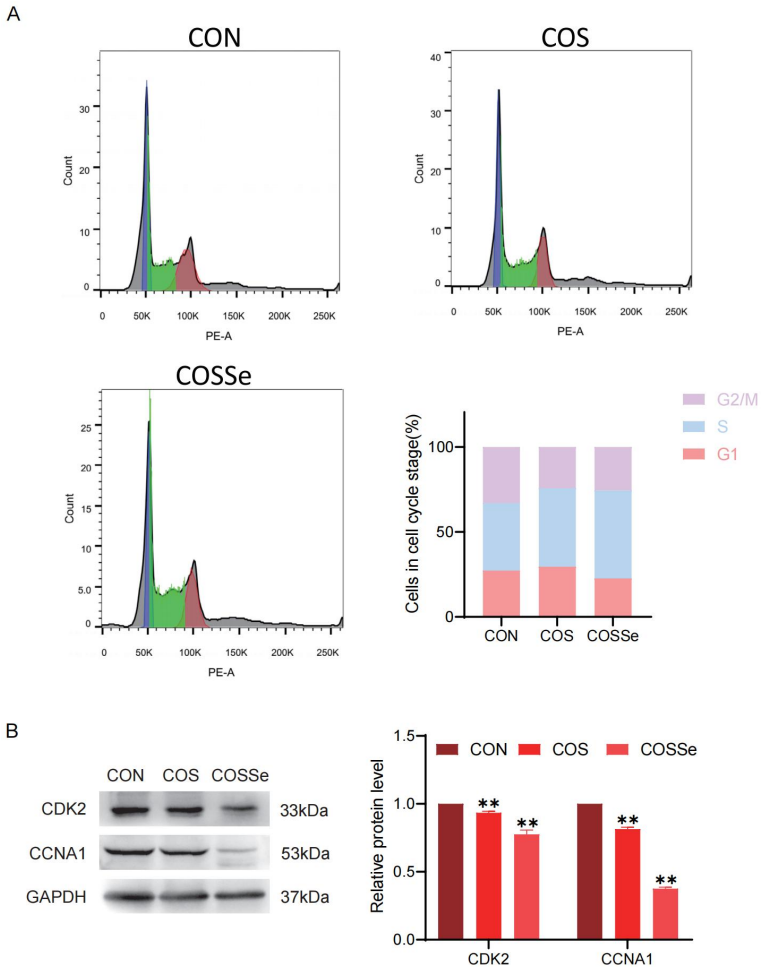

Figure 7 COS and COSSe alter the cell cycle of SKOV3. (A) Image of cell cycle outcome after COS and COSSe exposure detected by flow cytometry and statistics of cell cycle detection results that compared with the control group. (B) The expression of CDK2, CCNA1 in cells was detected by western blotting. The results were showed as mean ± SEM (n ≥ 3); $^{**}P < 0.01$ vs. the control group. CON, Control; COSSe, chitosan oligosaccharide selenium; COS, chitosan oligosaccharide.

RNA-seq results showed that COS and COSSe significantly altered the expression of the *SKOV3* gene with significant effects. In KEGG enrichment analysis, we found that both COS and COSSe affected the cell cycle and cell senescence progression of SKOV3 cells. In GO: BP enrichment analysis, we found that both COS and COSSe affected SKOV3 functions, such as ribonucleoprotein complex biogenesis, cytoplasmic translation, and ribosome biogenesis. We further performed functional enrichment analysis of the DEGs in COSSe and COS groups and found that they were related to DNA metabolic process and cell cycle. The cell cycle is a fundamental process in life that regulates mitosis and the formation of two daughter cells. The core of this process is regulated by CDK2 [23]. CDK abnormalities have been reported to cause proliferation and genomic and chromosomal instability, which leads to human cancer, and to promote cancer progression and aggressiveness [24]. CDK2, a central cell cycle regulator, is active from the late G1 phase through the entire S phase, and its activation involves binding with cyclin E1 (CCNE1) or E2, cyclin A2 (CCNA2), phosphorylation by the CDK activating kinase (CAK) complex, and the inhibitory removal of phosphorylation by cell division cycle 25 A (CDC25A) [25]. Related studies have shown that if the expression of CCNA in cells is inhibited, resulting in the downregulation of bound CDK2 expression, the cell cycle will be arrested in the S phase [26]. Previous studies showed that melanophore involucrate polysaccharide induced cell cycle arrest in the S phase, triggered cell apoptosis, and inhibited the migration and invasion of OC cells [27]. *Astragalus* polysaccharides can promote the apoptosis of nasopharyngeal carcinoma cells, increase the number of cells in the G0/G1 and S phases, decrease the number of cells in the G2/M phase, and inhibit the migration and invasion of nasopharyngeal carcinoma cells [28]. Horsetail alga could induce apoptosis and arrest the cell cycle in the S phase of melanoma cells [29]. Our study showed that both COS and COSSe could inhibit the formation of CCNA1-CDK2 complex by inhibiting the expression of CCNA1-CDK2 complex, mediate cell cycle arrest in the S phase, and thus inhibit cell proliferation, and the inhibitory effect of COSSe was stronger than that of COS. In conclusion, the results of the present study indicate that COS and COSSe inhibit the proliferation of SKOV3 cells by blocking the cycle of SKOV3 cells in the S phase, and COSSe has a stronger inhibitory effect.

References

1. Zheng Y, Yan JY, Cao CY, Liu YF, Yu DP, Liang XM. Application of chromatography in purification and structural analysis of natural polysaccharides: A review. *J Sep Sci.* 2023;46(18):e2300368. Available at: http://doi.org/10.1002/jssc.202300368
2. Yu Y, Shen M, Song Q, Xie J. Biological activities and pharmaceutical applications of polysaccharide from natural resources: A review. *Carbohydr Polym.* 2018;183:91–101. Available at: http://doi.org/10.1016/j.carbpol.2017.12.009
3. Mallakpour S, Azadi E, Hussain CM. Recent advancements in synthesis and drug delivery utilization of polysaccharides-based nanocomposites: The important role of nanoparticles and layered double hydroxides. *Int J Biol Macromol.*

2021;193:183–204. Available at: http://doi.org/10.1016/j.ijbiomac.2021.10.123
4. Mohammed ASA, Naveed M, Jost N. Polysaccharides; classification, chemical properties, and future perspective applications in fields of pharmacology and biological medicine (A review of current applications and upcoming potentialities). *J Polym Environ.* 2021;29(8):2359–2371. Available at: http://doi.org/10.1007/s10924-021-02052-2
5. Li J, Shen BX, Nie SL, Duan ZH, Chen KS. A combination of selenium and polysaccharides: promising therapeutic potential. *Carbohydr Polym.* 2019;206:163–173. Available at: http://doi.org/10.1016/j.carbpol.2018.10.088
6. Roman M, Jitaru P, Barbante C. Selenium biochemistry and its role for human health. *Metallomics.* 2014;6(1):25–54. Available at: http://doi.org/10.1039/C3MT00185G
7. Duntas LH, Benvenga S. Selenium: an element for life. *Endocrine.* 2014;48(3):756–775. Available at: http://doi.org/10.1007/s12020-014-0477-6
8. Hadrup N, Ravn-Haren G. Absorption, distribution, metabolism and excretion (ADME) of oral selenium from organic and inorganic sources: A review. *J Trace Elem Med Biol.* 2021;67:126801. Available at: http://doi.org/10.1016/j.jtemb.2021.126801
9. Gao X. Editorial: selenium and human health. *Front Nutr.* 2023;10. Available at: http://doi.org/10.3389/fnut.2023.1269204
10. Huang SY, Yang WJ, Huang GL. Preparation and activities of selenium polysaccharide from plant such as Grifola frondosa. *Carbohydr Polym.* 2020;242:116409. Available at: http://doi.org/10.1016/j.carbpol.2020.116409
11. Wei DF, Chen T, Yan MF, et al. Synthesis, characterization, antioxidant activity and neuroprotective effects of selenium polysaccharide from Radix hedysari. *Carbohydr Polym.* 2015;125:161–168. Available at: http://doi.org/10.1016/j.carbpol.2015.02.029
12. Jiang ZW, Chi JH, Li H, Wang YT, Liu WS, Han BQ. Effect of chitosan oligosaccharide-conjugated selenium on improving immune function and blocking gastric cancer growth. *Eur J Pharmacol.* 2021;891:173673. Available at: http://doi.org/10.1016/j.ejphar.2020.173673
13. Liu XG, Gao YX, Li DQ, et al. The neuroprotective and antioxidant profiles of selenium-containing polysaccharides from the fruit of Rosa laevigata. *Food Funct.* 2018;9(3):1800–1808. Available at: http://doi.org/10.1039/C7FO01725A
14. Chen SF, Zhou YQ, Chen YR, Gu J. Fastp: an ultra-fast all-in-one FASTQ preprocessor. *Bioinformatics.* 2018;34(17):i884–i890. Available at: https://doi.org/10.1093/bioinformatics/bty560
15. Zhang FL, Feng YQ, Wang JY, et al. Single cell epigenomic and transcriptomic analysis uncovers potential transcription factors regulating mitotic/meiotic switch. *Cell Death Dis.* 2023;14(2):134. Available at: http://doi.org/10.1038/s41419-023-05671-w
16. Li WF, Ma HH, Yuan S, Zhang XF. Production of pyracantha polysaccharide-iron(III) complex and its biologic activity. *Molecules.* 2021;26(7):1949. Available at: http://doi.org/10.3390/molecules26071949
17. Feng G, Zhang XF. Production of a codonopsis polysaccharide iron complex and evaluation of its properties. *Int J Biol Macromol.* 2020;162:1227–1240. Available at: http://doi.org/10.1016/j.ijbiomac.2020.06.210
18. Liu M, Jing H, Zhang J, et al. Optimization of mycelia selenium polysaccharide extraction from agrocybe cylindracea SL-02 and assessment of their antioxidant and anti-ageing activities. *PLoS One.* 2016;11(8):e0160799. Available at: http://doi.org/10.1371/journal.pone.0160799
19. Zhang Y, Khan MZH, Yuan T, et al. Preparation and characterization of D. opposita Thunb polysaccharide-zinc inclusion complex and evaluation of anti-diabetic activities. *Int J Biol Macromol.* 2019;121:1029–1036. Available at: http://doi.org/10.1016/j.ijbiomac.2018.10.068
20. Liu X, Wu ZF, Guo CJ, et al. Hypoxia responsive nano-drug delivery system based on angelica polysaccharide for liver cancer therapy. *Drug Deliv.* 2021;29(1):138–148. Available at: http://doi.org/10.1080/10717544.2021.2021324
21. Yan YY, Yuan S, Ma HH, Zhang XF. Structural modification and biological activities of carboxymethyl Pachymaran. *Food Sci Nutr.* 2021;9(8):4335–4348. Available at: http://doi.org/10.1002/fsn3.2404
22. Xiao H, Chen C, Li C, Huang Q, Fu X. Physicochemical characterization, antioxidant and hypoglycemic activities of selenized polysaccharides from Sargassum pallidum. *Int J Biol Macromol.* 2019;132:308–315. Available at: http://doi.org/10.1016/j.ijbiomac.2019.03.138
23. Schafer KA. The cell cycle: a review. *Vet Pathol.* 1998;35(6):461–478. Available at: http://doi.org/10.1177/030098589803500601
24. Malumbres M, Barbacid M. Cell cycle kinases in cancer. *Curr Opin Genet Dev.* 2007;17(1):60–65. Available at: http://doi.org/10.1016/j.gde.2006.12.008
25. Patra D, Bhavya K, Ramprasad P, Kalia M, Pal D. Anti-cancer drug molecules targeting cancer cell cycle and proliferation. *Adv Protein Chem Struct Biol.* 2023;135:343–395. Available at: http://doi.org/10.1016/bs.apcsb.2022.11.011
26. Kudo T, Ikeda M, Nishikawa M, et al. The RASSF3 candidate tumor suppressor induces apoptosis and G1-S cell-cycle arrest via p53. *Cancer Res.* 2012;72(11):2901–2911. Available at: http://doi.org/10.1158/0008-5472.CAN-12-0572
27. Qu JY, He YM, Shi Y, et al. Polysaccharides derived from Balanophora polyandra significantly suppressed the proliferation of ovarian cancer cells through P53-mediated pathway. *J Cell Mol Med.* 2020;24(14):8115–8125. Available at: http://doi.org/10.1111/jcmm.15468
28. Yang YL, Lin ZW, He PT, Nie H, Yao QY, Zhang SY. Inhibitory effect of Astragalus polysaccharide combined with cisplatin on cell cycle and migration of nasopharyngeal carcinoma cell lines. *Biol Pharm Bull.* 2021;44(7):926–931. Available at: http://doi.org/10.1248/bpb.b20-00959
29. Xu F, Ding HM, Liu ZF, et al. Polysaccharide extracted from the Sargassum fusiforme induces cell cycle arrest and apoptosis of B16F10 melanoma cells through the PI3K/AKT pathway. *Mol Biol Rep.* 2023;50(8):6517–6528. Available at: http://doi.org/10.1007/s11033-023-08570-7